

# Quantum criticality in the metal-superconductor transition of interacting Dirac fermions on a triangular lattice

Yuichi Otsuka,<sup>1,\*</sup> Kazuhiro Seki,<sup>1,2,3</sup> Sandro Sorella,<sup>1,2,4</sup> and Seiji Yunoki<sup>1,3,5</sup>

<sup>1</sup>*Computational Materials Science Research Team,*

*RIKEN Center for Computational Science (R-CCS), Kobe, Hyogo 650-0047, Japan*

<sup>2</sup>*SISSA – International School for Advanced Studies, Via Bonomea 265, 34136 Trieste, Italy*

<sup>3</sup>*Computational Condensed Matter Physics Laboratory, RIKEN, Wako, Saitama 351-0198, Japan*

<sup>4</sup>*Democritos Simulation Center CNR–IOM Istituto Officina dei Materiali, Via Bonomea 265, 34136 Trieste, Italy*

<sup>5</sup>*Computational Quantum Matter Research Team,*

*RIKEN Center for Emergent Matter Science (CEMS), Wako, Saitama 351-0198, Japan*

(Dated: July 20, 2018)

We investigate a semimetal-superconductor phase transition of two-dimensional Dirac electrons at zero temperature by large-scale and essentially unbiased quantum Monte Carlo simulations for the half-filled attractive Hubbard model on the triangular lattice, in the presence of alternating magnetic  $\pi$  flux, that is introduced to construct two Dirac points in the one-particle bands at the Fermi level. This phase transition is expected to describe quantum criticality of the chiral XY class in the framework of the Gross-Neveu model, where, in the ordered phase, the  $U(1)$  symmetry is spontaneously broken and a mass gap opens in the excitation spectrum. We compute the order parameter of the  $s$ -wave superconductivity and estimate the quasiparticle weight from the long-distance behavior of the single-particle Green's function. These calculations allow us to obtain the critical exponents of this transition in a reliable and accurate way. Our estimate for the critical exponents is in good agreement with those obtained for a transition to a Kekulé valence bond solid, where an emergent  $U(1)$  symmetry is proposed [Z.-X. Li *et al.*, Nat. Commun. **8**, 314 (2017)].

## I. INTRODUCTION

The Hubbard model with the Dirac dispersion has been intensively investigated in recent years, since it represents an ideal platform to study interaction-driven quantum phase transitions in a controllable way. Several decades ago, it was realized that the Hubbard model on the honeycomb lattice, the canonical lattice model for the interacting Dirac electrons, can be investigated with an unbiased numerical method, showing a quantum phase transition between a semimetal and an antiferromagnetic insulating phase at a finite value of the critical interaction strength,  $U_c/t > 0$  [1]. This is in contrast to the case of the square lattice, where the nesting instability yields a trivial  $U_c/t = 0$  [2]. This subject has attracted much attention especially after two different spin liquid phases were proposed in the Hubbard model on the honeycomb and the  $\pi$ -flux square lattices [3, 4]. Although subsequent studies have concluded that the spin liquid phases in these models are unlikely [5–10], this query has also been an opportunity to investigate the interaction-driven phase transition of the Dirac fermions by modern numerical and analytical techniques with a renewed interest, focusing on fermionic quantum criticality and universality classes.

Herbut and co-workers argued that the quantum criticality of the semimetal-antiferromagnetic transition of the Dirac fermions is described by the Gross-Neveu (GN) model [11–13]. More generally, in the framework of the

GN theory, it is known that there are three universality classes depending on the symmetries of the order parameters in the ordered phases, where, in all cases, the chiral symmetry is broken and a finite gap appears in the excitation spectrum [14]. Since this behavior is universal, it should be detected also in Dirac fermions lattice models relevant for condensed matter physics. Indeed, the universal quantum criticality of the semimetal-antiferromagnetic transition, i.e., the  $SU(2)$  symmetry breaking, corresponding to the chiral Heisenberg class in terms of the GN model, was numerically confirmed by calculating the critical exponents for the Hubbard model on the honeycomb lattice and on the square lattice with  $\pi$  flux [7–10]. On the other hand, the chiral Ising class, which describes the  $Z_2$  symmetry breaking in the interacting Dirac fermions, was examined in the charge-density-wave (CDW) transition of the spinless  $t$ - $V$  model on the same lattices [15–18]. In both cases, quantum Monte Carlo (QMC) methods, designed for the simple Hubbard-like lattice models, enable us to obtain the critical exponents with high accuracy, which was difficult by analytical methods based on renormalization-group (RG) approaches [13, 14, 19–24].

Among the three universality classes categorized by the GN theory, the remaining one, i.e., the chiral XY class corresponds to the  $U(1)$  symmetry breaking. For this class, the QMC results have been obtained on the basis of the Kekulé valence-bond-solid (VBS) transition [25, 26]. Although the Kekulé VBS state is naively understood as a consequence of the  $Z_3$  symmetry breaking, the RG arguments predict that the  $U(1)$  symmetry emerges at the quantum critical point because of peculiar gapless fermion fluctuations, implying that the Kekulé VBS tran-

\* [otsukay@riken.jp](mailto:otsukay@riken.jp)

sition belongs to the chiral XY class [25, 27–29]. The emergent  $U(1)$  symmetry was indeed observed in the QMC simulations [25, 26]. However, since it occurs only at the critical point, the scaling region can be significantly narrow, which may affect the QMC estimates of the critical exponents. Therefore, it is desirable to provide an independent estimate based on a lattice model where only the  $U(1)$  symmetry is present. Moreover the fermion anomalous dimension has not been obtained by the QMC method, yet.

In this paper, we study the quantum criticality of the chiral XY class on the basis of a lattice model which directly exhibits the  $U(1)$  symmetry breaking. Specifically, the attractive Hubbard model on the triangular lattice with alternating  $\pi$  flux at half electron filling is investigated by large-scale QMC simulations. In this model, the attractive on-site interaction drives the semimetal phase, which is stable in the weak-coupling region, to the  $s$ -wave superconducting (SC) phase where the  $U(1)$  symmetry is broken. We calculate the order parameter of the  $s$ -wave SC phase with high accuracy on lattices containing up to 2500 sites. The phase transition is also examined from the long-distance behavior of the single-particle Green's function, from which the quasiparticle weight is estimated. The critical exponents are obtained by a careful finite-size scaling analysis applied to these quantities. The critical point  $U_c/t$  and the correlation-length exponent  $\nu$ , estimated independently from the SC order parameter and the quasiparticle weight, show a good agreement, which clearly supports the quality of our calculation.

The rest of the paper is organized as follows. In the next section, we define the model and briefly explain the simulation method. The results of the SC order parameter and the quasiparticle weight are shown in Sec. III. The obtained exponents are compared with the previous results before concluding the paper in Sec. IV.

## II. MODEL AND METHOD

### A. Model

The attractive Hubbard model is expressed by the following Hamiltonian:

$$H = \sum_{\langle i,j \rangle, \sigma} t_{ij} (c_{i\sigma}^\dagger c_{j\sigma} + \text{h.c.}) - U \sum_i n_{i\uparrow} n_{i\downarrow}, \quad (1)$$

where  $c_{i\sigma}^\dagger$  creates an electron with spin  $\sigma (= \uparrow, \downarrow)$  at site  $i$ , located at  $\mathbf{r}_i = i_x \mathbf{e}_x + i_y \mathbf{e}_y$  on the triangular lattice ( $i_x$  and  $i_y$ : integer) [see Fig. 1(a)], and  $n_{i\sigma} = c_{i\sigma}^\dagger c_{i\sigma}$ . The sum indicated by  $\langle i, j \rangle$  runs over all pairs of neighboring sites  $i$  and  $j$  on the triangular lattice. The first term represents the kinetic energy defined by the tight-binding model with the transfer integrals  $t_{ij} = -|t_{ij}| e^{i\theta_{ij}}$ . We consider the model with uniform  $|t_{ij}| = t$  for both links of the triangular lattice, as depicted by

solid and dashed lines in Fig. 1(a). The magnetic  $\pi$  flux is imposed for every other triangle, which is realized by choosing  $\theta_{ij} = \pi$  for the dashed links. Owing to this flux pattern, the noninteracting energy dispersion,  $\varepsilon_{\mathbf{k}}^\pm = \pm 2t \sqrt{1 + \cos^2(k_x + k_y) + \cos^2 k_x - \cos^2 k_y}$ , has two Dirac points at  $\mathbf{K} = (\pm\pi/2, 0)$ , as shown in Fig. 1(b). The second term in Eq. (1) represents the attractive interaction ( $U > 0$ ), which induces the phase transition to the  $s$ -wave SC phase with increasing  $U$ . We study the model at half filling where the Fermi level is located at the Dirac points ( $\varepsilon_{\mathbf{k}=\mathbf{K}}^\pm = 0$ ); thus the low-lying excitations are described by the spin-1/2 Dirac fermions [30].

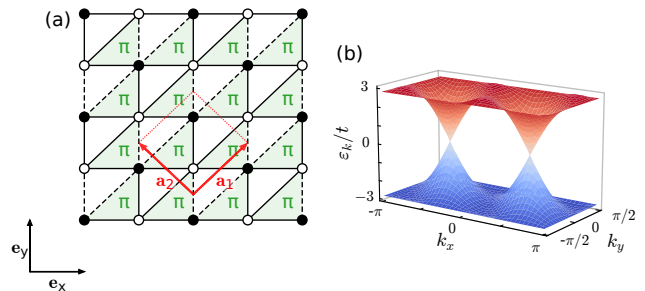


FIG. 1. (a) Lattice structure of the triangular lattice with alternating  $\pi$  flux. Each unit cell spanned by the primitive translational vectors (red arrows),  $\mathbf{a}_1 = (1, 1)$  and  $\mathbf{a}_2 = (-1, 1)$ , contains two sites indicated by solid and open circles, where the lattice constant is set to be one.  $\mathbf{e}_x = (1, 0)$  [ $\mathbf{e}_y = (0, 1)$ ] is the unit vector along the  $x$  ( $y$ ) direction. Transfer integrals for solid and dashed lines are  $-t$  and  $-te^{i\pi}$ , respectively. The phase factor for the dashed line leads to a magnetic  $\pi$  flux penetrating through each shaded triangle. (b) Energy dispersion in the noninteracting limit ( $U/t = 0$ ). The Fermi level is located at  $\varepsilon_{\mathbf{k}}/t = 0$  for half filling.

In contrast to the  $\pi$ -flux model on the square lattice [8–10, 31–33], the sublattice symmetry is absent in our model because of the triangular-lattice geometry. This indicates that the model (1) itself does not satisfy the chiral symmetry. In the noninteracting limit, the effective low-energy Hamiltonian is obtained by a linear expansion in  $\delta\mathbf{k} = \mathbf{k} - \mathbf{K} = (\delta k_x, \delta k_y)$ , as

$$H_{\text{eff}} = \pm 2t \delta k_x \sigma_x + 2t \delta k_y \sigma_y \mp 2t (\delta k_x + \delta k_y) \sigma_z, \quad (2)$$

where  $\boldsymbol{\sigma} = (\sigma_x, \sigma_y, \sigma_z)$  represent the Pauli matrices. We notice that the usual chiral operator  $\sigma_z$  does not anticommute with the effective Hamiltonian,  $\{H_{\text{eff}}, \sigma_z\} = H_{\text{eff}} \sigma_z + \sigma_z H_{\text{eff}} \neq 0$ , since Eq. (2) has the nonzero  $\sigma_z$  term. However, we can still define a general chiral operator as  $\gamma = \mathbf{n}_\gamma \cdot \boldsymbol{\sigma}$  with  $\gamma^2 = \sigma_0$ , where  $\sigma_0$  is a  $2 \times 2$  unit operator, satisfying the condition of the chiral symmetry at the Dirac points [34]. For the specific case of Eq. (2), it is easily shown that  $\{H_{\text{eff}}, \gamma\} = 0$  holds for a choice of  $\mathbf{n}_\gamma = (\pm 1, 1, \pm 1)/\sqrt{3}$ , which implies that the chiral symmetry is retained in the vicinity of the Dirac points in the continuum limit. We thus expect that the critical behavior near the phase transition is effectively described

by the GN theory, because only the Dirac dispersion near the Fermi level is relevant in the low-energy limit of the model (1).

On the other hand, depending on the presence or absence of the sublattice symmetry, different symmetries are broken at strong coupling. On the square lattice at half filling, the SC phase transition is accompanied by the CDW transition resulting in the  $SU(2)$  symmetry breaking [35, 36], whereas only the SC phase transition, i.e., the  $U(1)$  symmetry breaking, occurs on the triangular lattice [37, 38].

We study the model (1) from a theoretical point of view without considering its origin or a possible candidate for material realization. However, let us point out that, owing to recent technological developments in manipulating atoms trapped in optical lattices, it has become possible to introduce the staggered  $\pi$  flux in triangular lattices [39]. Since interactions between atoms in the optical lattices are also tunable [40], the transitions studied in this work might be experimentally explored in the near future.

## B. Method

Since the attractive Hubbard model is free from the negative sign problem [2], we adopt the ground-state projection within the auxiliary-field QMC method [41, 42]. In this technique, an expectation value of a physical observable  $O$  is calculated as

$$\langle O \rangle = \lim_{\tau \rightarrow \infty} \frac{\langle \psi_L | e^{-\frac{\tau}{2}H} O e^{-\frac{\tau}{2}H} | \psi_R \rangle}{\langle \psi_L | e^{-\tau H} | \psi_R \rangle}, \quad (3)$$

where  $\tau$  is a projection time and  $\langle \psi_L |$  ( $|\psi_R \rangle$ ) is a left (right) trial wave function having a finite overlap with the ground state. The Suzuki-Trotter decomposition [43, 44] is applied to the projection operator,  $e^{-\Delta\tau H} = e^{-\frac{1}{2}\Delta\tau H_0} e^{-\Delta\tau H_1} e^{-\frac{1}{2}\Delta\tau H_0} + \mathcal{O}(\Delta\tau^3)$ , where  $H_0$  ( $H_1$ ) represents the first (second) term in Eq. (1), and  $\Delta\tau = \tau/N_\tau$  with  $N_\tau$  being integer. In practice,  $\tau$  and  $N_\tau$  are not infinite but set large enough to have negligible systematic errors. In addition, since the QMC simulations are performed on finite-size clusters, the results are always affected by finite-size effects. This error can be systematically eliminated by performing simulations on large clusters and employing well established finite-size scaling analysis, as will be shown in the following section. The finite-size clusters used in this study are determined by two orthogonal lattice vectors ( $L_x \mathbf{e}_x, L_y \mathbf{e}_y$ ) with the same length  $L_x = L_y = L$  containing  $N = L^2$  sites [see Fig. 1(a)], and the periodic-boundary conditions are imposed along the  $x$  and  $y$  directions. On each cluster, we confirm that the systematic errors are sufficiently small compared to the statistical errors by choosing  $\tau = (L+4)/t$  and  $\Delta\tau = 0.1/t$ .

## III. RESULTS

In this section, we first confirm that the CDW order does not develop, while the SC order does in the strong coupling region. The  $s$ -wave SC order parameter is obtained from a simple extrapolation of the correlation function as a function of  $1/L$ , which gives a rough estimation of the phase boundary  $U_c/t$  and the critical exponent for the order parameter  $\beta$ . Then, by using a standard finite-size scaling analysis, we estimate  $U_c/t$  and  $\beta$  more accurately and also obtain the correlation-length exponent  $\nu$ . We then examine the phase transition from the semimetallic region. The quasiparticle weight is evaluated from the long-distance behavior of the single-particle Green's function, which yields another independent estimation of  $U_c/t$  and  $\nu$ , and also the remaining independent exponent  $\eta_\psi$ .

### A. Absence of the CDW order

Before discussing the numerical results, let us consider our model in the strong-coupling limit by a simple argument. The attractive Hubbard model is mapped onto the repulsive model under a partial (spin-down) particle-hole transformation [45, 46],

$$c_{i\uparrow} \rightarrow \tilde{c}_{i\uparrow} \quad (4)$$

$$c_{i\downarrow} \rightarrow \tilde{c}_{i\downarrow}^\dagger = (-1)^{s_i} c_{i\downarrow}, \quad (5)$$

where  $s_i = i_x + i_y$  and hence  $(-1)^{s_i}$  yields 1 ( $-1$ ) for sites depicted by open (solid) circles in Fig. 1(a). Since the triangular lattice is not bipartite, the kinetic term is not invariant under this transformation: In the mapped Hamiltonian, the signs of transfer integrals along the diagonal bonds in the square lattice representation, as shown in Fig. 1(a), are all spin dependent [38]. Therefore, in the strong-coupling limit, the effective spin model for the mapped repulsive model has an XXZ-type anisotropy, which is given by

$$\tilde{H}_{\text{eff}} = \sum_{\langle i,j \rangle} \{ J_{ij}^z S_i^z S_j^z + J_{ij}^{xy} (S_i^x S_j^x + S_i^y S_j^y) \}, \quad (6)$$

where  $S_i^\alpha$  is the spin-1/2 operator of the localized electron described by  $\tilde{c}_{i\sigma}$  and  $J_{ij}^\alpha$  denotes the neighboring spin interaction due to the second-order kinetic processes. Since  $J_{ij}^z = 4t^2/U \equiv J > 0$  for all the bonds in each triangle, the antiferromagnetic order in the  $z$  direction, which corresponds to the CDW order in the language of the original attractive Hubbard model, is strongly suppressed because of the geometrical frustration.

On the other hand, the order in the  $xy$  plane, corresponding to  $s$ -wave SC order in the attractive Hubbard model, is not prevented, because  $J_{ij}^{xy} = J$  between the nearest-neighboring sites and  $J_{ij}^{xy} = -J$  for the second-neighboring diagonal bond in the square lattice representation [Fig. 1(a)]. Therefore, we expect only the  $s$ -wave SC order, i.e., the  $U(1)$  symmetry breaking, in the

strong-coupling region, and thus the model studied here is particularly appropriate to examine the genuine  $U(1)$  universality class of the GN transition.

We numerically confirm the above argument by directly calculating the CDW correlation function,

$$P_{\text{CDW}}(L) = \frac{1}{N} \sum_{i,j} (-1)^{s_i+s_j} \langle (n_{i\uparrow} + n_{i\downarrow}) (n_{j\uparrow} + n_{j\downarrow}) \rangle, \quad (7)$$

from which the CDW order parameter is obtained as  $m_{\text{CDW}} = \lim_{L \rightarrow \infty} \sqrt{P_{\text{CDW}}(L)/N}$ . We define two sequences of clusters,  $L = 4n$  and  $L = 4n + 2$ , with  $n$  being integer. The difference is that, with the periodic-boundary conditions, the former has the Dirac points among the allowed momenta and the latter does not. The system sizes studied are  $L = 8, 12, 16, 20, 24, 32, 40, 48$  (this sequence of clusters denoted in the following as “ $L_{4n}$ ”) and  $L = 10, 14, 18, 22, 26, 34, 42, 50$  (this sequence of clusters denoted in the following as “ $L_{4n+2}$ ”), respectively. As shown in Fig. 2, the CDW order parameter clearly vanishes in both sequences of clusters  $L_{4n}$  and  $L_{4n+2}$ .

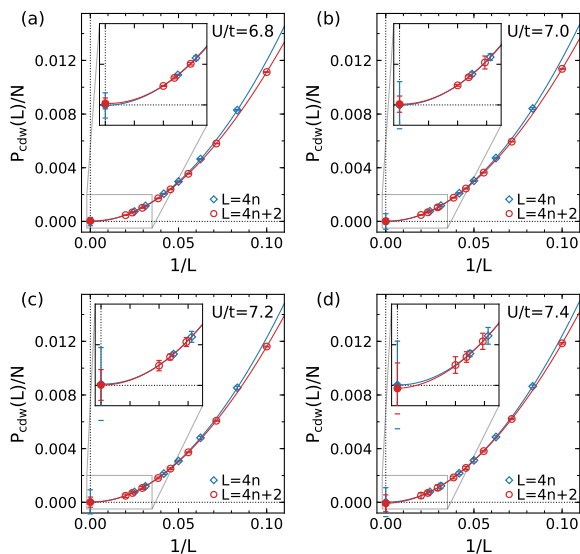


FIG. 2. CDW correlation function  $P_{\text{CDW}}(L)$  extrapolated to the thermodynamic limit for (a)  $U/t = 6.8$ , (b)  $U/t = 7.0$ , (c)  $U/t = 7.2$ , and (d)  $U/t = 7.4$ . Open diamonds (circles) represent results for  $L = 4n$  ( $L = 4n + 2$ ). Solid curves are least-square fits to the data with cubic polynomials in  $1/L$ . Insets show enlarged plots for large  $L$ . The extrapolated values in the thermodynamics limit are shown by filled symbols at  $1/L = 0$ .

## B. SC order parameter

Next, we calculate the  $s$ -wave pairing correlation function,

$$P_s(L) = \frac{1}{N} \sum_{i,j} \langle c_{i\uparrow}^\dagger c_{i\downarrow}^\dagger c_{j\downarrow} c_{j\uparrow} + c_{j\downarrow} c_{j\uparrow} c_{i\uparrow}^\dagger c_{i\downarrow}^\dagger \rangle, \quad (8)$$

on each finite-size cluster of the two sequences  $L_{4n}$  and  $L_{4n+2}$ . As shown in Fig. 3, these two sequences indeed show different finite-size behaviors especially for small  $L$  but converge to consistent values in the thermodynamics limit. Because of this different asymptotic behavior, it is not possible to apply the finite-size scaling analysis for the mixed data set with  $L_{4n}$  and  $L_{4n+2}$ . One may consider that the suitable choice should be  $L_{4n}$ ; it has the Dirac points in the allowed momenta, which is expected to be important in the long wavelength limit. However, in the practical QMC simulations, the sequence  $L_{4n+2}$  has the considerable advantage that the noninteracting model has a nondegenerate ground state  $|\psi_{U=0}\rangle$ , which is known as “closed-shell condition” [47]. This is particularly useful because one can select the trial wave functions as  $|\psi_L\rangle = |\psi_R\rangle = |\psi_{U=0}\rangle$ . This accelerates the convergence to the limit of  $\tau \rightarrow \infty$  (see discussion in Ref. 5) with much less computational effort since the spin-up determinant and the spin-down determinant are exactly the same in this case, and one needs to compute only one of them and with half the dimension corresponding to the  $L_{4n}$  case, allowing at least four times more efficient computations. For this reason, in the rest of the paper, we apply the finite-size scaling analysis only to the sequence of clusters with  $L = 4n + 2$ , for which we can obtain statistically accurate results up to the largest cluster of  $L = 50$ .

The order parameter  $\Delta_s$  of the  $s$ -wave SC phase is obtained by extrapolating  $P_s(L)$  in the thermodynamics limit, i.e.,  $\Delta_s = \lim_{L \rightarrow \infty} \sqrt{P_s(L)/N}$ , and the result is shown as a function of  $U/t$  in Fig. 4. The critical point,  $U_c/t$ , above which the SC order sets in, and the critical exponent are estimated by assuming a standard power-law behavior of this quantity close to  $U_c$  in the form of  $\Delta_s \sim (U - U_c)^\beta$ , where  $\beta$  is the critical exponent corresponding to the SC order parameter. Fitting with this form of  $\Delta_s$  evaluated from the simple-minded finite-size scaling, we find that there exists a rather large uncertainty, especially in  $\beta$ . Nevertheless, the result indicates that the transition is continuous. Therefore, we can apply much more effective and accurate methods to study the critical behavior.

To this end, we employ the standard method based on the “collapse fit” that uses all the data points both below and above  $U_c/t$ . This method is known to be very effective for second-order phase transitions. For the SC order parameter calculated on each finite-size cluster,  $\Delta_s(L, U) = \sqrt{P_s(L)/N}$ , we adopt the finite-size scaling relation,

$$\Delta_s(L, U) = L^{-\beta/\nu} f_s(uL^{1/\nu}), \quad (9)$$

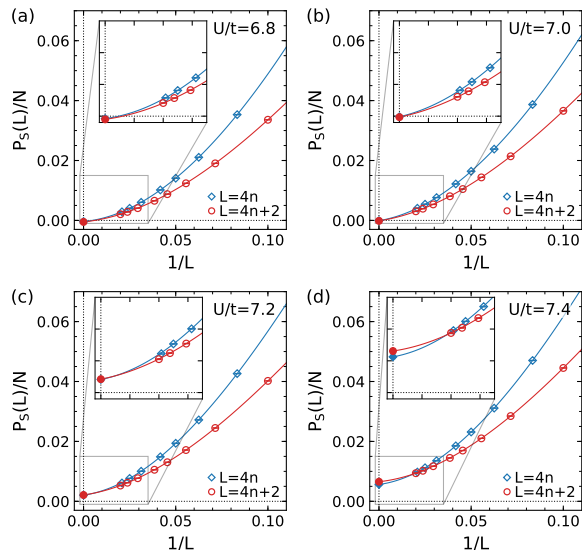


FIG. 3.  $s$ -wave pairing correlation function  $P_s(L)$  extrapolated to the thermodynamic limit for (a)  $U/t = 6.8$ , (b)  $U/t = 7.0$ , (c)  $U/t = 7.2$ , and (d)  $U/t = 7.4$ . Open diamonds (circles) represent results for  $L = 4n$  ( $L = 4n + 2$ ). Solid curves are least-square fits to the data with cubic polynomials in  $1/L$ . Insets show enlarged plots for large  $L$ . The extrapolated values are shown by filled symbols at  $1/L = 0$ .

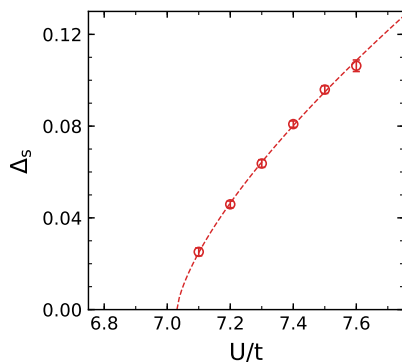


FIG. 4.  $s$ -wave SC order parameter  $\Delta_s$  as a function of  $U/t$  for  $L = 4n + 2$ . A dashed line is a least-square fit to the data points with the form of  $\Delta_s \sim (U - U_c)^\beta$ , from which the critical point and the exponent are estimated as  $U_c/t = 7.03(2)$  and  $\beta = 0.70(6)$ .

where  $u = (U - U_c)/U_c$  denotes the normalized interaction centered at the critical point, and  $f_s$  represents a scaling function. According to Eq. (9), the critical points and the exponents are determined by requiring that the data points of  $\Delta_s(L, U)L^{\beta/\nu}$  as a function of  $uL^{1/\nu}$  are tightly collapsed to a smooth function  $f_s$ , whose functional form is in general unknown. We employ a method based on Bayesian statistics to obtain tight data collapse in a wide range of  $uL^{1/\nu}$  [48]. The error bars are evaluated by a resampling technique: We generate several hundreds of replicas of the QMC data which are distributed

in accordance with the corresponding statistical errors and repeat the collapse fit for each replica with different initial parameters of  $U_c/t$ ,  $\nu$ , and  $\beta$ . The error bars are estimated as standard deviations in the distributions of the converged parameters [10]. A typical example of this procedure is shown in Fig. 5.

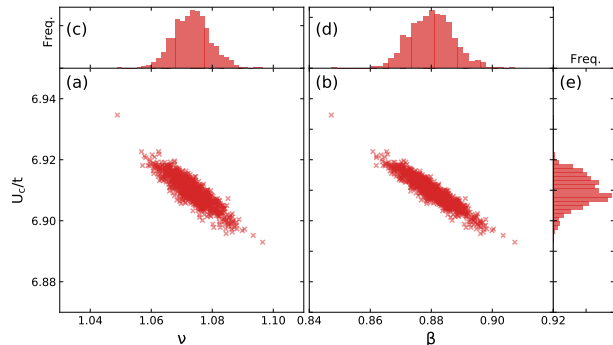


FIG. 5. (a),(b) Scattering plots and (c)-(e) histograms for the converged values of  $U_c/t$ ,  $\nu$ , and  $\beta$  in the resampling procedure for  $L_{\min} = 18$ .

The results of the data-collapse analysis are summarized in Table I. We check the finite-size effect by selecting different subsets of the data;  $L_{\min}$  denotes the smallest system size used in the data collapse (for example, the results for  $L = 18, 22, 26, 34, 50$  are used when  $L_{\min} = 18$ ). In general, one expects that the results converge to the exact values in the thermodynamics limit with increasing  $L_{\min}$ . This is the case notably when the corrections to the scaling relation are not negligible. However, since we do not observe a significant drift especially in the estimated values of  $U_c/t$  with increasing  $L_{\min}$ , we expect that our results obtained by the large-scale simulations have reached the asymptotic scaling regime governed by Eq.(9) without requiring therefore the corrections to scaling. On the other hand, the statistical errors become large for larger  $L_{\min}$ , because the number of data points in the fit decreases. Thus, as a compromise between reliability and accuracy, we set  $L_{\min} = 18$  to estimate the critical indices, and we obtain with this choice a well-collapsed fit, as shown in Fig. 6. The values of  $U_c/t$  ( $\beta$ ) obtained with this analysis are smaller (larger) than those estimated from the simple extrapolation adopted in Fig. 4. This is presumably because near the critical point it is difficult to determine a small value of the order parameter by the simple  $1/L$  extrapolation [7]. We also check that the data points of  $L_{4n}$  in Fig. 3 are fairly collapsed with these critical exponents.

### C. quasiparticle weight

We further examine the values of  $U_c/t$  and  $\nu$  from another physical observable in the semimetallic region. Recently, we have noticed that the quasiparticle weight can be evaluated from the equal-time single-particle Green's

TABLE I. Results of the critical point,  $U_c/t$ , and the exponents,  $\nu$  and  $\beta$ , obtained from data collapse of  $\Delta_s(L, U)$ .  $L_{\min}$  denotes the smallest system size used in data collapse. The number in each parenthesis indicates the statistical error, corresponding to the last digit of the value.

$L_{\min}$	$U_c/t$	$\nu$	$\beta$
10	6.915(3)	1.063(3)	0.870(3)
14	6.910(4)	1.070(4)	0.878(5)
18	6.910(5)	1.073(6)	0.880(7)
22	6.905(7)	1.08(1)	0.90(1)

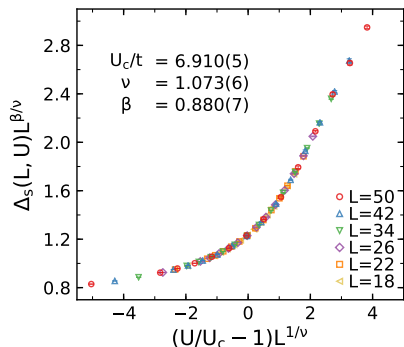


FIG. 6. Collapse fit of  $\Delta_s(L, U)$ . The critical point and exponents are determined in Table I for  $L_{\min} = 18$ .

function, which is the basic quantity and can be calculated with the highest accuracy within the auxiliary-field QMC method [49]. We consider the equal-time single-particle Green's function,

$$D(\mathbf{r}) = \sum_{\sigma} \langle c_{i\sigma}^{\dagger} c_{j\sigma} \rangle, \quad (10)$$

where sites  $i$  and  $j$  belong to different sublattices, indicated by solid and open circles in Fig. 1(a), and  $\mathbf{r} = \mathbf{r}_i - \mathbf{r}_j$ . Given that the Green's function near the Fermi level takes a Fermi-liquid-type form [50], it can be shown that the Green's function in the long-distance limit is expressed as

$$\lim_{|\mathbf{r}| \rightarrow \infty} D(\mathbf{r}) = Z \lim_{|\mathbf{r}| \rightarrow \infty} D^{(0)}(\mathbf{r}), \quad (11)$$

where  $Z$  denotes the quasiparticle weight [51–54] at the Fermi level and  $D^{(0)}(\mathbf{r})$  is the Green's function in the noninteracting limit. This relation follows from the fact that the long-distance propagation of a hole is determined by the zero-energy excitations at the Dirac points, where the amplitude of the hole is renormalized from 1 in the noninteracting limit to  $Z$ . One may expect that the Fermi velocity is renormalized by the interaction and thereby have some impact on the Green's function  $D(\mathbf{r})$ . However, it can also be shown that the renormalization of the Fermi velocity does not change Eq. (11), if the linear Dirac dispersion exists, which is expected at least within the semimetallic region [55]. More detailed dis-

cussions on the basis of the repulsive Hubbard model on the honeycomb lattice will be published elsewhere [49].

For a finite-size cluster, the quasiparticle weight is estimated as

$$Z(L, U) = \frac{D(\mathbf{r}_{\max})}{D^{(0)}(\mathbf{r}_{\max})}, \quad (12)$$

where the Green's functions are calculated at the maximum distance in the cluster,  $\mathbf{r} = \mathbf{r}_{\max}$ , so as to detect the power law behavior at long distance expected in the semimetallic phase. We perform data-collapse fits for this quantity based on the finite-size scaling relation,

$$Z(L, U) = L^{-\eta_{\psi}} f_Z(uL^{1/\nu}), \quad (13)$$

where  $\eta_{\psi}$  is the anomalous dimension of the fermion field, and  $f_Z$  is a scaling function. Following the same procedure as in the case of  $\Delta_s(L, U)$ , we obtain  $U_c/t$ ,  $\nu$ , and  $\eta_{\psi}$  in Table II. It is worth noting that  $U_c/t$  and  $\nu$  estimated by the two independent analyses (Tables I and II) almost coincide within two standard deviations. This is considered to be a nontrivial test for the accuracy of the calculations. The quality of the data collapse is also excellent, as shown in Fig. 7.

TABLE II. Results of the critical point,  $U_c/t$ , and the exponents,  $\nu$  and  $\eta_{\psi}$ , obtained from data collapse of  $Z(L, U)$ .  $L_{\min}$  denotes the smallest system size used in data collapse. The number in each parenthesis indicates the statistical error, corresponding to the last digit of the value.

$L_{\min}$	$U_c/t$	$\nu$	$\eta_{\psi}$
10	6.913(4)	1.036(4)	0.162(2)
14	6.896(5)	1.056(6)	0.154(2)
18	6.891(8)	1.06(1)	0.151(4)
22	6.89(1)	1.05(2)	0.154(6)

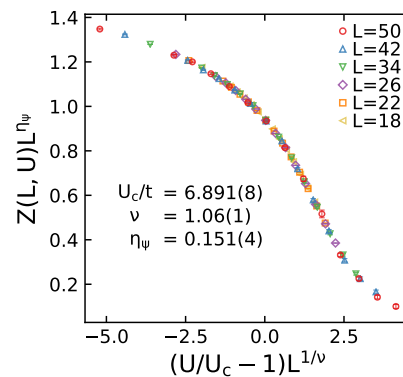


FIG. 7. Collapse fit of  $Z(L, U)$ . The critical point and exponents are determined in Table II for  $L_{\min} = 18$ .

#### IV. DISCUSSION AND CONCLUSIONS

In Table III, we compare our results with those obtained by the recent QMC simulations [25, 26] and RG approaches, such as the large- $N$  expansion [25, 56], the perturbative RG around the upper critical dimension  $d = 4 - \epsilon$  [14, 28], and the functional RG [29]. Remarkably, our results, both for  $\nu$  and  $\beta$ , agree well with the QMC results on different lattice models which exhibit the Kekulé VBS transition [25, 26]. Although the Kekulé VBS itself has the discrete  $Z_3$  symmetry breaking instead of  $U(1)$ , the RG arguments predict an emergent  $U(1)$  symmetry at the quantum-critical point because of gapless fermion fluctuations, suggesting that the quantum criticality of the Kekulé transition can be described in terms of the chiral XY universality class [25, 27, 29]. The agreement of the critical exponents between the Kekulé and the SC transitions, the latter showing a genuine  $U(1)$  symmetry breaking, strongly supports this scenario. The agreement may also indicate that corrections to scaling, which are predicted by the functional RG argument [29], turn out to be small in the Kekulé VBS transition.

On the other hand, we observe sizable differences between the QMC and the analytical estimates, as also previously noticed in the cases of the chiral Heisenberg [10, 28] and the chiral Ising universality classes [17, 28]. However, when compared to the recent higher-order calculations [28, 56] and the nonperturbative functional RG results [29], the discrepancies are rather small and systematic. Our estimate of  $\nu$  is always smaller than the analytical results by  $\lesssim 10\%$ . For  $\beta$ , the deviations are typically of the order of 20%. The most noticeable difference is found in  $\eta_\psi$ . For this quantity only the four-loop RG calculation [28] yields values comparable to our results but still  $\lesssim 30\%$  off. It is clear that further efforts are required both from the numerical and the analytical approaches to resolve the remaining discrepancies.

In conclusion, we have systematically studied the Dirac fermions with attractive interaction that allows us to examine the  $U(1)$  symmetry breaking, i.e., a genuine semimetal-superconductor transition without the CDW order, occurring at the finite value of the attractive interaction  $U_c$ . By performing large-scale QMC simulations on lattices containing up to 2,500 sites, we have pinned down the transition from the two different observables, i.e., the quasiparticle weight characterizing the semimetal for  $U \leq U_c$  and the  $s$ -wave pairing correlation function characterizing the superconductor for  $U \geq U_c$ . From these quantities, we have obtained consistent val-

ues of  $U_c$  and correlation-length exponent  $\nu$ . Together with the other exponents,  $\beta$  and  $\eta_\psi$ , determined also in this study, our results provide a complete description of the quantum criticality for the chiral XY class in the GN theory. Our results represent a useful benchmark calculation for future study of superconductor phase transitions in condensed matter physics and for an exhaustive classification of critical phenomena in quantum field theory models, such as the GN model.

TABLE III. Critical exponents,  $\nu$ ,  $\beta$ , and  $\eta_\psi$ , for the chiral XY class. QMC results (upper four rows) are based on lattice models, while analytical results (shown in the remaining rows) are obtained for the GN model. The first (second) row represents the results from the analysis of  $\Delta_s(L, U)$  [ $Z_s(L, U)$ ] with  $L_{\min} = 18$ . Two results for the fourth order of the  $4 - \epsilon$  expansion are calculated by different Padé approximations. The values of  $\beta$  which are not directly available in the references [14, 25, 26, 28, 29] are calculated from the values of the boson anomalous dimension  $\eta_\phi$  and the correlation-length exponent  $\nu$  using the scaling relation  $\beta = \frac{1}{2}\nu(1 + \eta_\phi)$ .

Method	$\nu$	$\beta$	$\eta_\psi$
QMC (present)	1.073(6)	0.880(7)	...
QMC (present)	1.06(1)	...	0.151(4)
QMC [25]	1.06(5)	0.90(6)	...
QMC [26]	1.05(5)	0.92(5)	...
Large- $N$ , 1st order [25]	1.25	0.75	0.083
Large- $N$ , higher orders [56]	1.11	1.05	0.0872
$4 - \epsilon$ , 1st order [14]	0.726	0.619	0.071
$4 - \epsilon$ , 2nd order [14]	0.837	0.705	0.063
$4 - \epsilon$ , 4th order [28]	1.19	1.08	0.117
$4 - \epsilon$ , 4th order [28]	1.19	1.06	0.108
functional RG [29]	1.16	1.09	0.062

#### ACKNOWLEDGMENTS

We acknowledge J. Goryo, Y. Hatsugai, and S. Ryu for valuable comments. This work has been supported in part by Grant-in-Aid for Scientific Research from MEXT Japan (under Grant Nos. 26400413 and 18K03475), RIKEN iTHES Project, MIUR-PRIN-2010. The numerical simulations have been performed on K computer provided by the RIKEN Center for Computational Science (R-CCS) through the HPCI System Research project (Project IDs: hp160159, hp170162, and hp170328), and RIKEN supercomputer system (HOKUSAI GreatWave). K. S. acknowledges support from JSPS Overseas Research Fellowships.

[1] S. Sorella and E. Tosatti, “Semi-Metal-Insulator Transition of the Hubbard Model in the Honeycomb Lattice,” *Europhys. Lett.* **19**, 699 (1992).

[2] J. E. Hirsch, “Two-dimensional Hubbard Model: Numerical Simulation Study,” *Phys. Rev. B* **31**, 4403 (1985).

[3] Z. Y. Meng, T. C. Lang, S. Wessel, F. F. Assaad, and A. Muramatsu, “Quantum Spin Liquid Emerging in Two-Dimensional Correlated Dirac Fermions,” *Nature* **464**, 847 (2010).

[4] C.-C. Chang and R. T. Scalettar, “Quantum Disordered Phase near the Mott Transition in the Staggered-Flux

- Hubbard Model on a Square Lattice,” *Phys. Rev. Lett.* **109**, 026404 (2012).
- [5] S. Sorella, Y. Otsuka, and S. Yunoki, “Absence of a Spin Liquid Phase in the Hubbard Model on the Honeycomb Lattice,” *Sci. Rep.* **2**, 992 (2012).
- [6] S. R. Hassan and David Sénéchal, “Absence of Spin Liquid in Nonfrustrated Correlated Systems,” *Phys. Rev. Lett.* **110**, 096402 (2013).
- [7] F. F. Assaad and I. F. Herbut, “Pinning the Order: The Nature of Quantum Criticality in the Hubbard Model on Honeycomb Lattice,” *Phys. Rev. X* **3**, 031010 (2013).
- [8] D. Ixert, F. F. Assaad, and K. P. Schmidt, “Mott Physics in the Half-Filled Hubbard Model on a Family of Vortex-Full Square Lattices,” *Phys. Rev. B* **90**, 195133 (2014).
- [9] F. Parisen Toldin, M. Hohenadler, F. F. Assaad, and I. F. Herbut, “Fermionic Quantum Criticality in Honeycomb and  $\pi$ -flux Hubbard Models: Finite-size Scaling of Renormalization-Group-Invariant Observables from Quantum Monte Carlo,” *Phys. Rev. B* **91**, 165108 (2015).
- [10] Y. Otsuka, S. Yunoki, and S. Sorella, “Universal Quantum Criticality in the Metal-Insulator Transition of Two-Dimensional Interacting Dirac Electrons,” *Phys. Rev. X* **6**, 011029 (2016).
- [11] D. Gross and A. Neveu, “Dynamical Symmetry Breaking in Asymptotically Free Field Theories,” *Phys. Rev. D* **10**, 3235 (1974).
- [12] I. F. Herbut, “Interactions and Phase Transitions on Graphene’s Honeycomb Lattice,” *Phys. Rev. Lett.* **97**, 146401 (2006).
- [13] I. F. Herbut, V. Juričić, and O. Vafek, “Relativistic Mott Criticality in Graphene,” *Phys. Rev. B* **80**, 075432 (2009).
- [14] B. Rosenstein and A. Kovner, “Critical Exponents of New Universality Classes,” *Phys. Lett. B* **314**, 381 (1993).
- [15] L. Wang, P. Corboz, and M. Troyer, “Fermionic Quantum Critical Point of Spinless Fermions on a Honeycomb Lattice,” *New J. Phys.* **16**, 103008 (2014).
- [16] Z.-X. Li, Y.-F. Jiang, and H. Yao, “Fermion-Sign-Free Majorana-Quantum-Monte-Carlo Studies of Quantum Critical Phenomena of Dirac Fermions in Two Dimensions,” *New J. Phys.* **17**, 085003 (2015).
- [17] S. Hesselmann and S. Wessel, “Thermal Ising Transitions in the Vicinity of Two-Dimensional Quantum Critical Points,” *Phys. Rev. B* **93**, 155157 (2016).
- [18] L. Wang, Y.-H. Liu, and M. Troyer, “Stochastic Series Expansion Simulation of the  $t$ - $V$  Model,” *Phys. Rev. B* **93**, 155117 (2016).
- [19] J. A. Gracey, “Three-Loop Calculations in the  $O(N)$  Gross-Neveu Model,” *Nucl. Phys. B* **341**, 403 (1990).
- [20] J. A. Gracey, “Computation of Critical Exponent  $\eta$  at  $O(1/N^3)$  in the Four-Fermi Model in Arbitrary Dimensions,” *Int. J. Mod. Phys. A* **09**, 727 (1994).
- [21] A. N. Vasil’ev, S. É. Derkachev, N. A. Kivel’, and A. S. Stepanenko, “The  $1/n$  Expansion in the Gross-Neveu Model: Conformal Bootstrap Calculation of the Index  $\eta$  in Order  $1/n^3$ ,” *Theor. Math. Phys.* **94**, 127 (1993).
- [22] L. Rosa, P. Vitale, and C. Wetterich, “Critical Exponents of the Gross-Neveu Model from the Effective Average Action,” *Phys. Rev. Lett.* **86**, 958 (2001).
- [23] F. Höfling, C. Nowak, and C. Wetterich, “Phase Transition and Critical Behavior of the  $d = 3$  Gross-Neveu Model,” *Phys. Rev. B* **66**, 205111 (2002).
- [24] L. Janssen and I. F. Herbut, “Antiferromagnetic Critical Point on Graphene’s Honeycomb Lattice: A Functional Renormalization Group Approach,” *Phys. Rev. B* **89**, 205403 (2014).
- [25] Z.-X. Li, Y.-F. Jiang, S.-K. Jian, and H. Yao, “Fermion-induced quantum critical points,” *Nat. Commun.* **8**, 314 (2017).
- [26] X. Y. Xu, K. T. Law, and P. A. Lee, “Kekulé valence bond order in an extended Hubbard model on the honeycomb lattice, with possible applications to twisted bilayer graphene,” *arXiv:1805.00478*.
- [27] M. M. Scherer and I. F. Herbut, “Gauge-field-assisted Kekulé quantum criticality,” *Phys. Rev. B* **94**, 205136 (2016).
- [28] N. Zerf, L. N. Mihaila, P. Marquard, I. F. Herbut, and M. M. Scherer, “Four-loop critical exponents for the Gross-Neveu-Yukawa models,” *Phys. Rev. D* **96**, 096010 (2017).
- [29] L. Classen, I. F. Herbut, and M. M. Scherer, “Fluctuation-induced continuous transition and quantum criticality in Dirac semimetals,” *Phys. Rev. B* **96**, 115132 (2017).
- [30] The spin liquid phase was found in the repulsive model on the same lattice by variational cluster approximation [57].
- [31] I. Affleck and J. B. Marston, “Large- $n$  Limit of the Heisenberg-Hubbard Model: Implications for High- $T_c$  Superconductors,” *Phys. Rev. B* **37**, 3774 (1988).
- [32] I. Affleck, Z. Zou, T. Hsu, and P. W. Anderson, “SU(2) Gauge Symmetry of the Large- $U$  Limit of the Hubbard Model,” *Phys. Rev. B* **38**, 745 (1988).
- [33] Y. Otsuka and Y. Hatsugai, “Mott Transition in the Two-Dimensional Flux Phase,” *Phys. Rev. B* **65**, 073101 (2002).
- [34] Y. Hatsugai, “Topological aspect of graphene physics,” *J. Phys. Conf. Ser.* **334**, 012004 (2011).
- [35] R. T. Scalettar, E. Y. Loh, J. E. Gubernatis, A. Moreo, S. R. White, D. J. Scalapino, R. L. Sugar, and E. Dagotto, “Phase diagram of the two-dimensional negative-  $U$  Hubbard model,” *Phys. Rev. Lett.* **62**, 1407 (1989).
- [36] A. Moreo and D. J. Scalapino, “Two-dimensional negative-  $U$  Hubbard model,” *Phys. Rev. Lett.* **66**, 946 (1991).
- [37] R. R. dos Santos, “Second-neighbor hopping in the attractive Hubbard model,” *Phys. Rev. B* **46**, 5496 (1992).
- [38] R. R. dos Santos, “Attractive Hubbard model on a triangular lattice,” *Phys. Rev. B* **48**, 3976 (1993).
- [39] J. Struck, C. Ölschläger, M. Weinberg, P. Hauke, J. Simonet, A. Eckardt, M. Lewenstein, K. Sengstock, and P. Windpassinger, “Tunable Gauge Potential for Neutral and Spinless Particles in Driven Optical Lattices,” *Phys. Rev. Lett.* **108**, 225304 (2012).
- [40] L. Hackermüller, U. Schneider, M. Moreno-Cardoner, T. Kitagawa, T. Best, S. Will, E. Demler, E. Altman, I. Bloch, and B. Paredes, “Anomalous expansion of attractively interacting fermionic atoms in an optical lattice,” *Science* **327**, 1621 (2010).
- [41] R. Blankenbecler, D. J. Scalapino, and R. L. Sugar, “Monte Carlo Calculations of Coupled Boson-Fermion Systems. I,” *Phys. Rev. D* **24**, 2278 (1981).
- [42] S. R. White, D. J. Scalapino, R. L. Sugar, E. Y. Loh, J. E. Gubernatis, and R. T. Scalettar, “Numerical Study of the Two-Dimensional Hubbard Model,” *Phys. Rev. B* **40**,



- 506 (1989).
- [43] M. Suzuki, “Generalized Trotter’s Formula and Systematic Approximants of Exponential Operators and Inner Derivations with Applications to Many-Body Problems,” *Commun. Math. Phys.* **51**, 183 (1976).
- [44] H. F. Trotter, “On the Product of Semi-Groups of Operators,” *Proc. Amer. Math. Soc.* **10**, 545 (1959).
- [45] H. Shiba, “Thermodynamic Properties of the One-Dimensional Half-Filled-Band Hubbard Model. II,” *Prog. Theor. Phys.* **48**, 2171 (1972).
- [46] V. J. Emery, “Theory of the quasi-one-dimensional electron gas with strong “on-site” interactions,” *Phys. Rev. B* **14**, 2989 (1976).
- [47] S. Sorella, “Finite-size scaling with modified boundary conditions,” *Phys. Rev. B* **91**, 241116 (2015).
- [48] K. Harada, “Bayesian Inference in the Scaling Analysis of Critical Phenomena,” *Phys. Rev. E* **84**, 056704 (2011).
- [49] K. Seki, Y. Otsuka, S. Yunoki, and S. Sorella, (unpublished).
- [50] A. A. Abrikosov, L. P. Gor’kov, and I. E. Dzyaloshinski, *Methods of quantum field theory in statistical physics* (Dover Publications, New York, 1975).
- [51] A. B. Migdal, “The Momentum Distribution of Interacting Fermi Particles,” *Sov. Phys. JETP* **5**, 333 (1957).
- [52] J. M. Luttinger, “Analytic properties of single-particle propagators for many-fermion systems,” *Phys. Rev.* **121**, 942–949 (1961).
- [53] P. Nozières and J. M. Luttinger, “Derivation of the Landau theory of Fermi liquids. i. formal preliminaries,” *Phys. Rev.* **127**, 1423–1431 (1962).
- [54] J. M. Luttinger and P. Nozières, “Derivation of the Landau theory of Fermi liquids. ii. equilibrium properties and transport equation,” *Phys. Rev.* **127**, 1431–1440 (1962).
- [55] The noncriticality of the Fermi velocity has been confirmed in Refs [10](#), [58](#), and [59](#).
- [56] J. A. Gracey, “Large N critical exponents for the chiral Heisenberg Gross-Neveu universality class,” *Phys. Rev. D* **97**, 105009 (2018).
- [57] S. Rachel, M. Laubach, J. Reuther, and R. Thomale, “Quantum Paramagnet in a  $\pi$  Flux Triangular Lattice Hubbard Model,” *Phys. Rev. Lett.* **114**, 167201 (2015).
- [58] I. F. Herbut, V. Juričić, and B. Roy, “Theory of Interacting Electrons on the Honeycomb Lattice,” *Phys. Rev. B* **79**, 085116 (2009).
- [59] W. Wu and A.-M. S. Tremblay, “Phase Diagram and Fermi Liquid Properties of the Extended Hubbard Model on the Honeycomb Lattice,” *Phys. Rev. B* **89**, 205128 (2014).